Nanocomposite Catalysts

Deutsche Ausgabe: DOI: 10.1002/ange.201602878
Internationale Ausgabe: DOI: 10.1002/anie.201602878

Synthesis of α-MoC_{1-x} Nanoparticles with a Surface-Modified SBA-15 Hard Template: Determination of Structure–Function Relationships in Acetic Acid Deoxygenation

Frederick G. Baddour, Connor P. Nash, Joshua A. Schaidle, and Daniel A. Ruddy**

Abstract: *Surface modification of mesoporous SBA-15 silica generated a hydrophobic environment for a molybdenum diamine (Mo-diamine) precursor solution, enabling direct growth of isolated 1.9 ± 0.4 nm α-MoC_{1-x} nanoparticles (NPs) inside the pores of the support. The resulting NP catalysts are bifunctional, and compared to bulk α-MoC_{1-x} and β-Mo_2C, the NPs exhibit a greater acid-site:H-site ratio and a fraction of stronger acid sites. The greater acid-site:H-site ratio results in higher decarbonylation (DCO) selectivity during acetic acid hydrodeoxygenation (HDO) reactions, and the stronger acid sites lead to higher activity and ketonization (KET) selectivity at high temperatures. The hard-templating synthetic method could be a versatile route toward carbide NPs of varying size, composition, and phase, on a range of mesoporous oxide supports.*

Ex situ catalytic fast pyrolysis (CFP) of biomass is a promising route to production of renewable liquid hydrocarbon fuels that are infrastructure compatible and cost competitive.[1] By immediately upgrading the pyrolysis vapors prior to condensation, this process aims to simultaneously stabilize the bio-oil product, while enhancing its fuel properties with hydrogenation, deoxygenation, and C–C coupling reactions. The realization of these goals will require new catalysts that possess bifunctional properties (that is, acidic and metallic sites), such that they can activate H_2 under low pressure, high temperature conditions, and favor cleavage of C–O bonds over C–C bonds.[2] Early transition-metal carbides are one class of materials that possess these bifunctional properties, and in particular, β-Mo_2C has received attention from our laboratory and others as an effective hydrodeoxygenation (HDO) catalyst for acetic acid, acetone, C_{2-3} alcohols and aldehydes, and anisole.[3] Our research identified the acid-site:H-site ratio as a key property that is influenced by surface termination, and if this property is tunable by composition, crystal phase, and/or particle size, the resulting deoxygenation performance may be controlled.

Molybdenum carbide (Mo-C) catalysts have long been compared to noble metals because of their catalytic reactivity.[4] Over the past 20 years, colloidal syntheses of noble metal nanoparticles (NPs) have been extensively developed to control NP composition, size, and morphology, especially for the catalytically important sub-10 nm size regime. These synthetic advances have resulted in improved catalytic performance (activity and selectivity for example) and an understanding of fundamental structure–function relationships (for example, structure-sensitive reactions) that drive next-generation catalyst development.[5] Similar synthetic routes that enable size and morphology control of supported carbide NPs represent a significant challenge and have yet to be developed with similar precision. Bulk Mo-C catalysts, including high surface area materials, are typically prepared by high temperature carburization methods employing methane and hydrogen. Such syntheses offer little control of size and morphology, and as a result, structure–function relationships developed for noble metal NPs remain elusive for carbide NPs, where particle size has only recently been demonstrated to be a critical factor.[6] Therefore, there is a continuing need to develop versatile routes to prepare supported NP carbide catalysts that can lead to controlled composition, phase, size, and morphology. Here we report a synthetic route to isolate supported α-MoC_{1-x} NPs, and we compare their reactivity for acetic acid deoxygenation to that of the more commonly studied β-Mo_2C.

Recently, two methane- and hydrogen-free synthetic routes were reported that generate nanostructured Mo-C. The urea glass method employs an ethanolic solution of $MoCl_5$ as the molybdenum source and urea as the carbon source to generate a NP-β-Mo_2C product after high temperature reaction.[7] Similarly, multiple phases of NP-Mo-C can be produced by the high temperature reaction of an amine–metal–oxide composite, which was precipitated from an aqueous solution of $(NH_4)_6Mo_7O_{24}$ and an organic polyamine.[8] Although these two methods represent significant advances in NP-Mo-C synthesis, the products consist of fused NPs, so dispersion of the carbide and immobilization onto a support material for catalytic testing remains challenging.

Sub-10 nm NPs of oxides and metals may be effectively isolated if they are directly grown on a mesoporous hard template such as SBA-15 silica.[9] Aspects of the two recent carbide syntheses were attractive to us, with the goal of directly growing carbide NPs on a high surface area SBA-15 silica support. We envisioned that a $MoCl_5$ solution in ethanol containing a urea carbon source would enable impregnation into the pores of the mesoporous silica and allow controlled NP-Mo-C growth. However, urea is known to decompose by a complex pathway.[10] Initial attempts to control the production of carbide versus nitride with the urea:molybdenum ratio did not translate from the urea glass method to this hard template approach. The phenylenediamines employed in the

[*] Dr. F. G. Baddour, C. P. Nash, Dr. J. A. Schaidle, Dr. D. A. Ruddy
National Bioenergy Center, National Renewable Energy Laboratory
15013 Denver West Parkway, Golden, CO 80401 (USA)
E-mail: joshua.schaidle@nrel.gov
dan.ruddy@nrel.gov

Supporting information for this article can be found under: http://dx.doi.org/10.1002/anie.201602878.

amine–Mo–oxide synthesis were reported to selectively produce carbide phases, however, they have low solubility in water and require pH adjustment and precipitation to form the amine–Mo–oxide composite. In contrast, stable solutions of $MoCl_5$ and 4-chloro-*ortho*-phenylenediamine (4Cl-*o*-PDA) were formed in ethanol that could be used to impregnate the SBA-15.

Initially, we investigated the conversion of $MoCl_5$ and 4Cl-*o*-PDA into a NP-Mo-C product without SBA-15. A red-brown ethanol solution of $MoCl_5$ and 4Cl-*o*-PDA was transferred to a quartz boat and dried overnight at 50 °C. The Mo-diamine gel that formed was then heated at 100 °C h^{-1} to 850 °C and held for 4 h under flowing N_2, followed by natural cooling to ambient temperature. Once cool, the material was passivated under a flow of 1 % O_2/N_2 for at least 2 h. The resulting lustrous material exhibited broad X-ray diffraction (XRD) peaks indicative of a nanocrystalline material that matched the peak positions for a face-centered cubic (fcc) α-MoC_{1-x} structure (Figure 1 A). TEM images revealed quasi spherical NPs 4.2 ± 1.8 nm in diameter (Figure 1 B). The NP-MoC_{1-x} product appears to be contained within an amorphous carbon matrix that also contains residual nitrogen based on the XRD data, TEM images, and the high carbon and nitrogen content (48.8 wt % C, 3.28 wt % N). This initial experiment validated the combination of $MoCl_5$ and 4Cl-*o*-PDA in ethanol as a route to selectively form a NP-Mo-C material, without the need for urea or pH adjustment to promote precipitation of the precursor.

To translate this approach to a hard template, SBA-15 (750 $m^2 g^{-1}$, 6.2 nm pores; Supporting Information, Table S1) was impregnated with an ethanolic solution of $MoCl_5$ and 4Cl-*o*-PDA, resulting in a brown material. The dried Mo-diamine/SBA-15 precursor was reacted at 850 °C, permitted to cool, and then passivated. The resulting black material also exhibited broad XRD peaks consistent with nanocrystalline α-MoC_{1-x}, similar to that prepared without the SBA-15 template (Figure 1 A). TEM images revealed NPs of a similar size, but they were not inside the SBA-15 pores (Figure 1 C). Although SBA-15 did not appear to alter the transformation of the Mo-diamine precursor into α-MoC_{1-x} NPs, the resulting material was a physical mixture of SBA-15 and NP-MoC_{1-x} in a carbonaceous matrix.

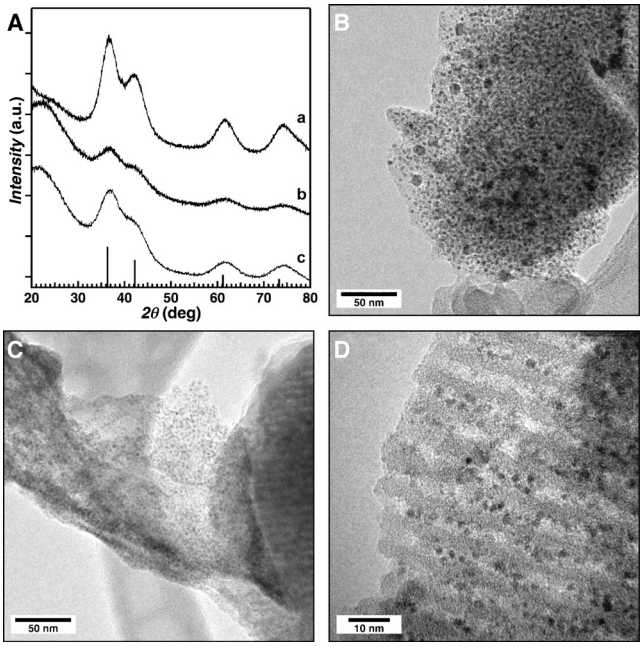

Figure 1. A) XRD patterns of NP-MoC_{1-x} materials: a) Untemplated NP-MoC_{1-x}, b) NP-Mo-C_{1-x} outside SBA-15, c) NP-MoC_{1-x}/mSBA, |) MoC (ICDD Card: 03-065-8092). TEM images for: B) untemplated NP-MoC_{1-x}, C) NP-MoC_{1-x} outside SBA-15 pores, and D) NP-MoC_{1-x}/mSBA.

The absence of MoC_{1-x} NPs inside the SBA-15 pores led us to suspect that the ethanolic Mo-diamine precursor solution did not effectively infiltrate the pores of the SBA-15 template during impregnation and/or did not remain in place during drying. The pores of SBA-15 silica are hydrophilic, possessing surface silanol groups.[11] Although the ethanolic Mo-diamine solution is considered hydrophilic, we hypothesized that the resulting Mo-4Cl-*o*-PDA species becomes increasingly hydrophobic upon drying and elimination of ethanol, leading to expulsion from the hydrophilic pores. Treatment of SBA-15 with Me_3SiNMe_2 at room temperature has been demonstrated to be particularly effective for generating a hydrophobic surface (that is, a 10-fold reduction in water adsorption), reacting with approximately 75 % of the available surface silanol groups.[11] Impregnation of a Me_3Si-modified SBA-15 (mSBA) with the same ethanol solution of $MoCl_5$ and 4Cl-*o*-PDA, followed by drying, reaction at 850 °C, and passivation, generated a black material (NP-MoC_{1-x}/mSBA) that exhibited broad XRD peaks consistent with nanocrystalline α-MoC_{1-x} (Figure 1 A). However, in this case TEM images revealed smaller NPs (1.9 ± 0.4 nm in diameter) immobilized inside the mSBA pores (Figure 1 D). After high temperature treatment, the SBA-15 hard template retained its mesoporous structure (4.8 nm pores), moderate surface area, and pore volume (250 $m^2 g^{-1}$, 0.23 cc g^-; Supporting Information, Table S1). The molybdenum loading for this material was 14.2 wt %, and similar to the untemplated NP-MoC_{1-x}, residual carbon and nitrogen were found by elemental analysis (20.6 wt % C, 1.12 wt % N).

In spite of the residual carbon and nitrogen residing in the templated and untemplated NP-MoC_{1-x} materials, both were found to possess H_2-activating and acid sites, as determined by H_2 chemisorption and ammonia temperature-programmed desorption (NH_3-TPD) after a 450 °C activation in flowing H_2. For comparison, bulk carbide materials were prepared by carburization of ammonium paramolybdate.[3a,12] When normalized to the amount of molybdenum in grams, both NP-MoC_{1-x} materials exhibited a density of H-sites comparable to bulk Mo_2C and a slightly increased density compared to bulk MoC_{1-x} (Table 1). The NP materials exhibit a significant increase in acid-site density (normalized to the amount of molybdenum in grams). The acid-site:H-site ratio for both NP-MoC_{1-x} materials was determined to be 18, which is greater than the ratio of 8.1 determined for bulk Mo_2C, and is slightly larger than that for bulk MoC_{1-x} (ratio of 14). The acid-site:H-site ratio seems to correlate with different crystal phases, α-MoC_{1-x} (fcc) versus β-Mo_2C (hcp). A further minor increase in acid-site:H-site ratio was observed for the

Table 1: H-sites determined by H_2 chemisorption, acid sites determined by NH_3-TPD, and acid-site:H-site ratio.

Material	H-sites [$\mu mol\, g_{Mo}^{-1}$]	Acid-sites [$\mu mol\, g_{Mo}^{-1}$]	Acid:H site ratio
Bulk Mo_2C	57	470	8.1
Bulk MoC_{1-x}	47	660	14
NP-MoC_{1-x}	62	1120	18
NP-MoC_{1-x}/mSBA	59	1060	18

NP-MoC_{1-x} materials. The acidity of Mo-C materials is associated with surface hydroxy groups,[3a,f] and recently, it was demonstrated that small β-Mo_2C NPs are more oxophilic than their larger counterparts.[6] Considering the similar oxophilicity of the small NPs reported herein, we attribute the observed increase in acid-site:H-site ratio resulting from size reduction, to an increased density of surface hydroxy groups. The NH_3-TPD profiles of the NP materials further highlight the differences in acid sites, and possess a pronounced high temperature shoulder that is not observed in the bulk materials, which exhibit a tailing desorption (Figure 2A). This high temperature contribution indicates the formation of additional acid sites with increased strength on the NP materials. Multi-peak fitting analysis and integration estimates that 12% of the acid sites on the NP materials correspond to these strong sites. Finally, a molybdenum-free control material, resulting from treatment of SBA-15 with 4Cl-*o*-PDA and heating at 850°C under flowing N_2, did not contribute to the acid- or H-site densities (Supporting Information, Figure S1).

Acetic acid (AA) is a major component of bio-oil and can undergo a variety of transformations, some of which incorporate H_2, making it an interesting probe molecule for bio-oil upgrading catalysts (Supporting Information, Table S2).[3a,13] Bulk and NP catalysts were investigated in the HDO of acetic acid under ex situ CFP conditions in a temperature-programmed reaction (TPRxn) after activation in flowing H_2. It should be noted that these TPRxn experiments do not measure steady-state rates, and therefore, reaction rates and product selectivities include the effects of deactivation and/or catalyst stabilization. Acetic acid and H_2 conversion rates were normalized to acid- and H-site densities, giving turnover rate (TOR) values (Figure 2B and C). Similar trends were observed when H_2 conversion rates were normalized to metal content (Supporting Information, Figure S2). The untemplated NP-MoC_{1-x} demonstrated the lowest TOR for both acetic acid and H_2, despite its high acid- and H-site densities. This low activity is attributed to the low surface area ($9.7\ m^2\, g^{-1}$) and low pore volume ($0.015\ cc\, g^{-}$) of this material (Supporting Information, Table S1). NP-MoC_{1-x}/mSBA (containing dispersed and isolated NPs in the mesopores) demonstrated a significantly greater acetic acid TOR than the untemplated NP-MoC_{1-x}, and similar TOR values compared to both bulk carbide materials below 400°C. Above 400°C, NP-MoC_{1-x}/mSBA demonstrated a greater acetic acid TOR than the bulk materials. In contrast, the H_2 TOR for NP-MoC_{1-x}/mSBA was approximately two-fold lower than that of the bulk catalysts throughout the temperature range explored. However, it is worth noting that the H_2 TOR is still an order of magnitude greater than the acetic acid TOR.

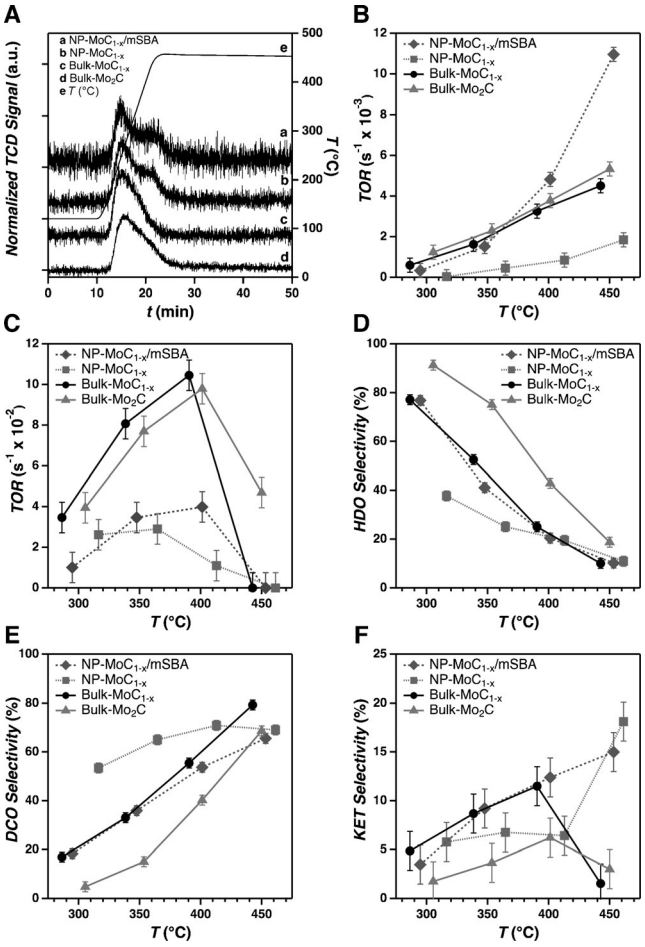

Figure 2. A) NH_3-TPD profiles, B) acetic acid TOR, C) hydrogen TOR, D) HDO selectivity, E) DCO selectivity, and F) KET selectivity.

Similar to bulk MoC_{1-x}, H_2 conversion dropped to zero at 450°C, and only bulk Mo_2C exhibited H_2 conversion at that temperature (Figure 2C). Finally, both NP catalysts contained residual chloride (1.40 wt%), which is often considered a catalyst poison but did not appear to adversely affect the catalytic performance of these materials.

Commonly observed pathways for acetic acid transformations under ex situ CFP conditions include, HDO, decarbonylation and decarboxylation (DCO), and ketonization (KET). For bifunctional bio-oil upgrading catalysts, HDO is particularly desirable to produce acetaldehyde, ethanol, ethylene, and ethane. Bulk Mo_2C has been reported to favor the HDO pathway over DCO and KET.[3a] Notably, although supported platinum catalysts are commonly compared to Mo-C materials, they strongly favor DCO of acetic acid under the aforementioned conditions (Supporting Information, Figure S3). Between 300–400°C, the selectivity of these carbide catalysts for HDO products (reported as the sum of carbon selectivities for acetaldehyde, ethanol, ethylene, and ethane) and DCO products (sum of carbon selectivity for CH_4, CO, and CO_2) is related to the acid-site:H-site ratio. Bulk Mo_2C, the catalyst with the lowest acid-site:H-site ratio, exhibited the highest HDO selectivity (Figure 2D). The MoC_{1-x} catalysts possess a greater acid-site:H-site ratio and exhibited

lower selectivity for HDO products and correspondingly greater selectivity for DCO products (Figure 2E). These data highlight the importance of the acid-site:H-site ratio for bifunctional catalysts, and support the concept that adjustment of this ratio will enable control over reaction selectivity.

The most notable difference in performance for the NP catalysts is increased KET selectivity (reported as carbon selectivity to acetone) with increased acetic acid TOR at high temperature. In contrast to bulk Mo_2C, all MoC_{1-x} catalysts exhibited a greater selectivity for KET products throughout the course of the TPRxn. The NP products exhibited significantly greater selectivity for this pathway at 450 °C (Figure 2F). The NP-MoC_{1-x}/mSBA catalyst demonstrated a 15 % selectivity for acetone at 450 °C. By comparison, the bulk carbides exhibited less than 3 % selectivity for acetone. A high acetic acid TOR was also observed at this temperature. The observed differences in selectivity and TOR for the NP-MoC_{1-x}/mSBA catalyst do not appear to be solely attributed to an increased acid-site:H-site ratio. Rather, the data suggest that the increased acetic acid TOR and KET selectivity at high temperature are a result of the fraction of stronger acid sites determined by NH_3-TPD that are not present on the bulk materials. The untemplated NP-MoC_{1-x} exhibits a similar high temperature KET selectivity (18 % at 450 °C). Active site access for acetic acid may be limited in the untemplated material, but similar selectivity is observed at the site. These high temperature data reveal the relationship between decreased particle size, increased acid strength, and a shift in the resulting catalytic performance towards KET.

To fully describe the surface species and the observed changes in site activity/selectivity of the NP catalysts, further experiments are necessary (for example, DRIFTS[3a]). However, these TPRxn results give preliminary evidence for the occurrence of structure–function relationships in Mo-C catalysts, where the phase/composition affects the acid-site:H-site ratio and the resulting HDO and DCO selectivities, and the particle size affects acid strength and the resulting KET activity/selectivity. Finally, the NP catalysts appear to be robust under these reaction conditions, exhibiting no phase changes in the XRD patterns, nor any obvious morphological changes or sintering in TEM images after TPRxn testing up to 600 °C (Supporting Information, Figure S4).

In summary, a synthetic route was developed for preparation of 1.9 nm NP-MoC_{1-x} by direct growth in the pores of a surface-modified, mesoporous SBA-15 hard template. This approach ensured that the hydrophobic Mo-4Cl-*o*-PDA precursor stayed within the mSBA pores, resulting in immobilization of discrete NPs of the carbide inside the pores. These NP-MoC_{1-x} materials possess both H_2-activating sites and acid sites, including a portion of stronger acid sites when compared to the bulk Mo-C materials. The preliminary structure–function relationships identified for this group of Mo-C catalysts make this NP synthetic method attractive for further development because it enables size and shape control by hard templates with varying pore sizes and morphologies. Furthermore, this method is potentially versatile, allowing NP carbide growth on supports that provide additional reactivity in deoxygenation reactions (for example, acidic, basic, or reducible oxide hard templates), and the exploration of carbides containing different metals (for example, WCl_6) and mixed-metal precursor solutions.

Acknowledgements

This work was supported by the Laboratory Directed Research and Development Program at the National Renewable Energy Laboratory and the Department of Energy Bioenergy Technologies Office under Contract no. DE-AC36-08-GO28308.

Keywords: bifunctional catalysts · biomass conversion · hydrodeoxygenation · metal carbides · surface chemistry

How to cite: *Angew. Chem. Int. Ed.* **2016**, *55*, 9026–9029
Angew. Chem. **2016**, *128*, 9172–9175

[1] A. Dutta, J. A. Schaidle, D. Humbird, F. G. Baddour, A. Sahir, *Top. Catal.* **2016**, *59*, 2–18.
[2] D. A. Ruddy, J. A. Schaidle, J. R. Ferrell III, J. Wang, L. Moens, J. E. Hensley, *Green Chem.* **2014**, *16*, 454–490.
[3] a) J. A. Schaidle, J. Blackburn, C. A. Farberow, C. Nash, K. X. Steirer, J. Clark, D. J. Robichaud, D. A. Ruddy, *ACS Catal.* **2016**, *6*, 1181–1197; b) S. K. Bej, L. T. Thompson, *Appl. Catal. A* **2004**, *264*, 141–150; c) M. M. Sullivan, A. Bhan, *ACS Catal.* **2016**, *6*, 1145–1152; d) H. Ren, W. Yu, M. Salciccioli, Y. Chen, Y. Huang, K. Xiong, D. G. Vlachos, J. G. Chen, *Green Chem.* **2014**, *16*, 761–769; e) M. M. Sullivan, J. T. Held, A. Bhan, *J. Catal.* **2015**, *326*, 82–91; f) W.-S. Lee, Z. Wang, R. J. Wu, A. Bhan, *J. Catal.* **2014**, *319*, 44–53; g) W.-S. Lee, A. Kumar, Z. Wang, A. Bhan, *ACS Catal.* **2015**, *5*, 4104–4114.
[4] a) S. T. Oyama, *Catal. Today* **1992**, *15*, 179–200; b) M. Lewandowski, A. Szymanska-Kolasa, P. Da Costa, C. Sayag, *Catal. Today* **2007**, *119*, 31–34.
[5] F. Zaera, *Chem. Soc. Rev.* **2013**, *42*, 2746–2762.
[6] D. R. Stellwagen, J. H. Bitter, *Green Chem.* **2015**, *17*, 582–593.
[7] a) C. Giordano, C. Erpen, W. Yao, M. Antonietti, *Nano Lett.* **2008**, *8*, 4659–4663; b) C. Giordano, C. Erpen, W. Yao, B. Milke, M. Antonietti, *Chem. Mater.* **2009**, *21*, 5136–5144.
[8] a) C. Wan, N. A. Knight, B. M. Leonard, *Chem. Commun.* **2013**, *49*, 10409–10411; b) C. Wan, Y. N. Regmi, B. M. Leonard, *Angew. Chem. Int. Ed.* **2014**, *53*, 6407–6410; *Angew. Chem.* **2014**, *126*, 6525–6528.
[9] a) E. Delahaye, V. Escax, N. El Hassan, A. Davidson, R. Aquino, V. Dupuis, R. Perzynski, Y. L. Raikher, *J. Phys. Chem. B* **2006**, *110*, 26001–26011; b) L. Zhao, J. Yu, *J. Colloid Interface Sci.* **2006**, *304*, 84–91; c) M. A. Ballem, F. Soderlind, P. Nordblad, P.-O. Kall, M. Oden, *Microporous Mesoporous Mater.* **2013**, *168*, 221–224; d) W. Zhu, Y. Han, L. An, *Microporous Mesoporous Mater.* **2005**, *80*, 221–226.
[10] a) P. M. Schaber, J. Colson, S. Higgins, D. Thielen, B. Anspach, J. Brauer, *Thermochim. Acta* **2004**, *424*, 131–142; b) I. V. Tokmakov, S. Alavi, D. L. Thompson, *J. Phys. Chem. A* **2006**, *110*, 2759–2770.
[11] R. L. Brutchey, D. A. Ruddy, L. K. Andersen, T. D. Tilley, *Langmuir* **2005**, *21*, 9576–9583.
[12] L. Volpe, M. Boudart, *J. Solid State Chem.* **1985**, *59*, 348–356.
[13] S. E. Habas, F. G. Baddour, D. A. Ruddy, C. P. Nash, J. Wang, M. Pan, J. E. Hensley, J. A. Schaidle, *Chem. Mater.* **2015**, *27*, 7580–7592.

Received: March 22, 2016
Published online: June 7, 2016

